Journal of Materials Chemistry C

ROYAL SOCIETY OF CHEMISTRY

PAPER

View Article Online
View Journal

Cite this: DOI: 10.1039/d5tc03684d

Performance enhancement of carbon dot-based luminescent solar concentrators *via* surface modification and TiO_2-enhanced scattering

Yunxiang Liu, Yoshiki Iso * and Tetsuhiko Isobe *

Carbon dots (CDs) are promising luminescent nanomaterials for a luminescent solar concentrator (LSC) due to facile synthesis, low toxicity, and environmental friendliness; to overcome the limitations of their moderate photoluminescence quantum yields (PLQYs) and photon utilization, in this work, tyramine-modified CDs (Tyr-CDs) were synthesized through a simple one-step surface modification at 250 °C under ambient conditions. After purification by silica gel column chromatography, the average particle size of Tyr-CDs was 32.1 ± 8.1 nm, while the excitation and emission wavelengths remained unchanged compared with unmodified CDs. Nevertheless, Tyr-CDs exhibited stronger UV and visible absorption and higher photoluminescence intensity. The PLQY increased from 56% to 68% through surface modification, which is attributed to the suppression of concentration quenching *via* steric hindrance that prevents π–π stacking. Embedding Tyr-CDs into ethylene–vinyl acetate (EVA) copolymer produced Tyr-CDs@EVA films, which exhibited improved optical properties compared with CDs@EVA film, which are prepared by embedding unmodified CDs into EVA. When applied to LSC devices, both short-circuit current and power conversion efficiency were significantly enhanced by surface modification with tyramine, which is consistent with the improved optical performance of Tyr-CDs@EVA film. In addition, Tyr-CDs/TiO_2@EVA film with a double EVA layer configuration containing individual Tyr-CDs and TiO_2 was prepared using 25.4 ± 6.7 nm TiO_2 nanoparticles. Compared with Tyr-CDs@EVA film, Tyr-CDs/TiO_2@EVA film further improved LSC performance owing to light scattering from TiO_2. Moreover, Tyr-CDs + TiO_2@EVA film, prepared by dispersing TiO_2 and Tyr-CDs together in EVA, achieved the highest power conversion efficiency due to volumetric light scattering.

Received 12th October 2025,
Accepted 20th December 2025

DOI: 10.1039/d5tc03684d

rsc.li/materials-c

1. Introduction

Luminescent solar concentrators (LSCs) have gained significant interest as cost-effective photovoltaic devices that enable efficient light harvesting and spectral conversion. They can be seamlessly integrated into building windows.[1] Luminescent materials in LSCs convert high-energy ultraviolet or visible photons into lower-energy visible or near-infrared photons. The converted light is directed to the waveguide edges through total internal reflection.[2] This minimizes optical losses and broadens the spectral response of solar cells. These characteristics not only enhance overall power conversion efficiency but also improve device stability and durability, making LSCs promising candidates for semi-transparent photovoltaic applications.[3,4] Nevertheless, the LSC performance strongly depends on the selection of luminescent materials and effective photon management within the device.

Luminescent materials are crucial for determining the LSC performance. The earliest luminophores applied in LSCs were organic dyes with high molar absorption coefficients and easily tunable optical properties.[5,6] However, photobleaching, narrow absorption bands, and limited long-term stability restrict their practical application.[7] Rare-earth complexes such as Eu^{3+} and Tb^{3+} exhibit high chemical stability.[8,9] Their luminescence efficiency and absorption coefficients are comparable to organic dyes, but are not as high as semiconductor quantum dots (QDs).[10,11] QDs, including CdSe/ZnS and $CsPbX_3$ (X = Cl, Br, I), have been widely studied for high photoluminescence quantum yields (PLQYs), tunable optical properties, and multicolor emission.[12–14] Nevertheless, high toxicity, complex synthesis, and environmental instability remain major obstacles to large-scale application.[15]

Carbon dots (CDs) are carbon-based nanomaterials that have recently attracted increasing attention as promising alternatives because of facile synthesis, low cost, low toxicity, and environmental friendliness.[16] CDs also exhibit broad absorption and

Department of Applied Chemistry, Faculty of Science and Technology, Keio University, 3-14-1 Hiyoshi, Kohoku-ku, Yokohama 223-8522, Japan.
E-mail: iso@applc.keio.ac.jp, isobe@applc.keio.ac.jp; Fax: +81 45 566 1551, +81 45 566 1551; Tel: +81 45 566 1558, +81 45 566 1554

Table 1 Surface-modified carbon dots (CDs) with PLQYs before and after modification

Precursor	Modification method	PLQY (before)	PLQY (after)	Year	Ref.
Glucose-derived CDs	Amine passivation with TTDDA	1%	13%	2009	23
Petroleum coke CDs	Hydrothermal treatment in ammonia solution (N-doping)	8.7%	15.8%	2014	24
Lamp black-derived CDs	Chemical reduction with $NaBH_4$/$LiAlH_4$	1.55%	7.25, 7.44%	2019	25
o-PD/urea-derived CDs	Acid treatment/thiourea doping/PEG passivation	36%	42%, 61%, 68%	2022	26
Lignin-derived CDs	Amination	3.4%	21.1%	2024	27
Lignin-derived CDs	Molecular modification of lignin precursor	5.36%	42.7%	2024	28
Citric acid + diaminonaphthalene	Surface amination (NH_3 + N_2H_4)	45%	70%	2020	29
p-PD-derived CDs	4-Morpholinoaniline surface modification	28.3%	41.8%	2022	30
p-PD-derived CDs	Surface modification with tyramine (250 °C, ambient)	56%	68%		This work

tunable photoluminescence (PL), making them attractive candidates for LSC applications.[17–21] However, the application of CDs in LSCs is still limited by their moderate PLQYs and concentration quenching effects, which reduce photon utilization and overall device efficiency.[22]

Surface modification has been employed to improve the optical properties of CDs, particularly by suppressing concentration quenching and thereby increasing PLQYs.[23–30] Modification strategies and their effects are summarized in Table 1. For instance, Liang *et al.* demonstrated that *o*-phenylenediamine/urea-derived CDs exhibited an increase in PLQY from 36% to 68% through acid treatment, thiourea doping, and polyethylene glycol modification, indicating the effectiveness of chemical treatment in enhancing PLQY.[26] Similarly, Sato *et al.* reported that surface-modified *p*-phenylenediamine(PD)-derived CDs in chloroform increased the PLQY from 28.3% to 41.8% owing to molecular functionalization.[30] Integrating modified CDs into LSC devices improves photon utilization. In addition, introducing light-scattering nanoparticles in LSCs can enhance photon utilization by redirecting incident light and luminescent light into the waveguide, thereby improving the efficiency of light-harvesting devices.[31,32] For example, Polché *et al.* demonstrated that embedding SiO_2 nanoparticles in CD-based films increased edge photon collection due to enhanced light scattering. This indicates the effectiveness of nanoparticle-assisted photon management,[31] which can also be applied to LSCs.

Our previous work demonstrated the facile one-step synthesis of high-PLQY CDs from *p*-PD under ambient conditions and the application in LSC devices.[33] In this work, to improve the PLQY, we modified *p*-PD-derived CDs with tyramine through a simple one-step process under ambient conditions to yield Tyr-CDs, as illustrated in Scheme 1. The purified Tyr-CDs were embedded in ethylene–vinyl acetate (EVA) copolymer to prepare Tyr-CDs@EVA film. We compared the optical properties and LSC performance of Tyr-CDs in chloroform and EVA with those of CDs reported in our previous work.[33] To further improve photon utilization, TiO_2 nanoparticles were used as a light scattering agent, and two types of composite films were prepared: Tyr-CDs/TiO_2@EVA film with a double EVA layer configuration containing individual Tyr-CDs and TiO_2, and Tyr-CDs + TiO_2@EVA film with a one EVA layer configuration containing a mixture of Tyr-CDs and TiO_2. The optical properties and LSC performance under AM1.5G simulated sunlight were systematically evaluated using soda glass as the light guide plate under different background color conditions, as shown in Scheme 2.

2. Experimental section

2.1. Materials

p-PD (>98.0%), tyramine (>98.0%), and 1-octadecene (>90.0%) were purchased from Tokyo Chemical Industry. Diphenyl ether (>99.0%), chloroform (>99.0%), hexane (>96.0%), dichloromethane (99.5%), methanol (>99.8%), and silica gel (100–210 μm neutral spherical particles) were purchased from Kanto Chemical. Granular EVA polymer (Evaflex® EV150) was purchased from DuPont-Mitsui Polychemicals. A free sample of TiO_2 powder AEROXIDE® TiO_2 NKT65 (specific surface area: 50 m^2 g^{-1}) was donated by Nippon Aerosil. All reagents were used as received without further purification.

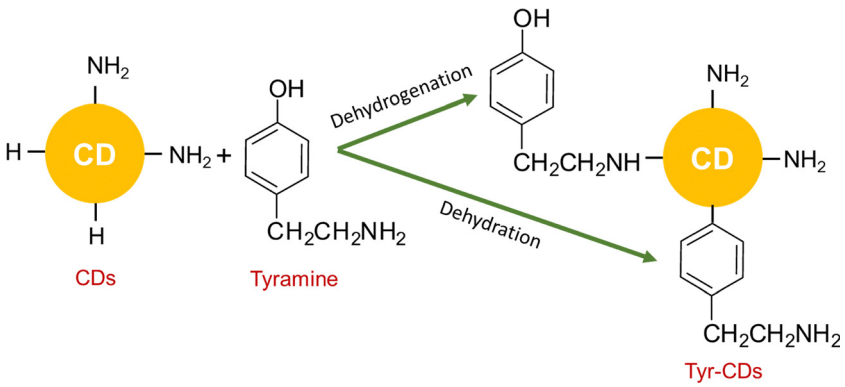

Scheme 1 Schematic illustration of the surface modification of CDs with tyramine to obtain Tyr-CDs.

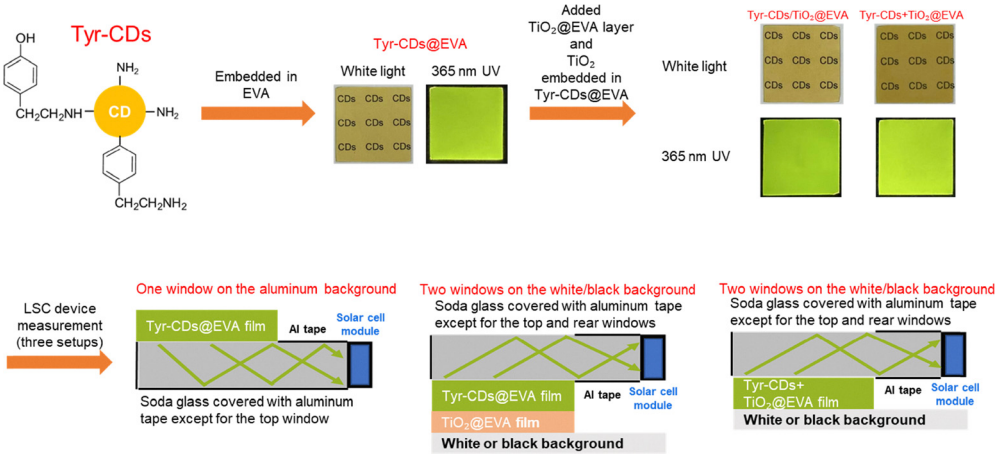

Scheme 2 Schematic illustration of the preparation of Tyr-CDs, Tyr-CDs/TiO_2@EVA, and Tyr-CDs + TiO_2@EVA films, and their evaluation in LSC devices under one-window and two-window conditions.

2.2. Synthesis of unmodified CDs and surface-modified CDs

The synthesis procedure of crude unmodified CDs was given below. *p*-PD (0.20 g, 1.85 mmol) was mixed with diphenyl ether (15 mL) and refluxed at 250 °C for 2 h under ambient air with magnetic stirring at 250 rpm conditions according to our previous work.[33] After cooling to room temperature, the resulting black suspension was divided into three equal parts and 33 mL of hexane was added to each. The mixtures were centrifuged at ~11 000*g* (10 cm radius rotor at 10 000 rpm) for 10 min. This step was repeated three times. Finally, all of the precipitates were mixed with methanol and then evaporated to obtain crude CDs.

Surface-modified CDs were synthesized following the same procedure as crude CDs, except for an additional post-modification step. After the initial 2 h reaction at 250 °C, the reaction system was naturally cooled to room temperature, and then a mixture of tyramine (0.126 g, 0.92 mmol) and diphenyl ether (7.5 mL), which had been pre-stirred for 1 h, was added to the reaction system. The mixture was further refluxed at 250 °C for 0.5 h under magnetic stirring at 250 rpm. After natural cooling to room temperature, the resulting black suspension was divided into three equal parts, and 33 mL of hexane was added to each. The mixtures were centrifuged at ~11 000 g (10 cm radius rotor at 10 000 rpm) for 10 min, and this step was repeated five times to remove the increased amount of diphenyl ether in the post-modification system. Finally, all of the precipitates were mixed with methanol and then evaporated to obtain crude Tyr-CDs.

2.3. Purification of crude CDs and Tyr-CDs through silica gel column chromatography

The crude Tyr-CDs were completely dispersed in an eluent with a volume ratio of dichloromethane to methanol of 20 : 1 and then purified using silica gel column chromatography (see Fig. S1, SI). The non-fluorescent fraction 1, mainly consisting of yellow components under white light, was removed first. The eluent ratio was then changed to 2 : 1, and the pale blue-emitting fraction 2 and the strongly red-emitting fraction 3, which consisted of red components under white light, were collected. Finally, the solvent in fraction 3 only was removed using a rotary evaporator and air-dried overnight at room temperature to obtain purified Tyr-CDs. The purification of crude CDs was performed using the same procedure as described above.[33]

The product yields, calculated from the weight ratio of purified CDs and Tyr-CDs to *p*-PD, were 25% and 11%, respectively. The crude CDs weighed 154 mg and yielded 50 mg after silica gel column purification, while the crude Tyr-CDs weighed 62 mg and yielded 21 mg after the same purification. These results indicate that the difference in yield mainly results from the formation stage of the crude product rather than from the purification process. Accordingly, the lower Tyr-CDs yield is likely due to the additional tyramine reaction. To improve the product yield, the reaction conditions need to be optimized, for example by using catalysts.[39] Purified CDs and Tyr-CDs (1 mg each) were dispersed in respective chloroform (40 mL) under ultrasonication for 10 min to obtain the chloroform dispersions of CDs and Tyr-CDs (25 mg L^{-1}) for analysis.

2.4. Fabrication of EVA, CDs@EVA, Tyr-CDs@EVA, TiO_2@EVA, Tyr-CDs/TiO_2@EVA, and Tyr-CDs + TiO_2@EVA films

2.4.1. EVA film. The granular EVA (2.6 g), chloroform (30 mL), and 1-octadecene (1.5 mL) were mixed and stirred at room temperature for 1 h to obtain an EVA solution. The EVA solution was then purged with Ar for 5 min, followed by stirring and defoaming using a planetary centrifugal mixer (Thinky, AR-100) for 30 s each. Finally, the EVA solution (5 mL) was cast into a Petri dish (inner diameter 4.86 cm) and left to dry for 36 h under ambient conditions to obtain EVA film.

2.4.2. CDs@EVA and Tyr-CDs@EVA films. To fabricate the CDs@EVA and Tyr-CDs@EVA films at a concentration of 0.05 wt%, the purified CDs and Tyr-CDs (1.3 mg each) were mixed with the respective EVA solutions (30 mL) mentioned in 2.4.1. After stirring for 24 h, each mixture was further dispersed ultrasonically for 1 h. In the same way as the EVA solution, the dispersions (15 mL) were cast to obtain CDs@EVA and Tyr-CDs@EVA films.

2.4.3. TiO_2@EVA film. To fabricate the TiO_2@EVA films at the concentrations of 0.05 wt%, 0.10 wt%, and 0.15 wt%, the TiO_2 powders (1.3 mg, 2.6 mg, and 3.9 mg, respectively) were each dispersed in the EVA solutions (30 mL) by magnetic stirring for 24 h followed by ultrasonication for 1 h. In the same way as the EVA solution, the dispersions (5 mL) were cast to obtain TiO_2@EVA films with different TiO_2 concentrations.

2.4.4. Tyr-CDs/TiO_2@EVA film. The Tyr-CD dispersion (15 mL) mentioned in 2.4.2 was cast onto the surface of each TiO_2@EVA film in a Petri dish, and further left to dry for 36 h under ambient conditions to obtain Tyr-CDs/TiO_2@EVA films.

2.4.5. Tyr-CDs + TiO_2@EVA film. To fabricate the Tyr-CDs + TiO_2@EVA films, 1.3 mg of Tyr-CDs and 3.9 mg of TiO_2 were added to the EVA solution (30 mL). In the same way as the EVA solution, the dispersions (15 mL) were cast to obtain Tyr-CDs + TiO_2@EVA film.

All films were cut into square pieces (35 mm × 35 mm). The thickness of the films was measured using a micrometer.

2.5. Characterizations

The particle size and morphology of Tyr-CDs and TiO_2 were imaged using a field emission transmission electron microscope (FE-TEM; FEI, Tecnai G2) operated at 200 kV. The FE-TEM samples were prepared by dropping a small amount of the Tyr-CDs and TiO_2 chloroform dispersions on copper grids with ultra-thin carbon support films (Oken Shoji, UHR-C10) and drying them overnight. Fourier transform infrared (FT-IR) spectra of samples in pressed KBr pellets were measured using a FT-IR spectrometer (JASCO, FT/IR-4200). The ultraviolet-visible (UV-vis) absorption spectra of dispersions were measured using a UV-vis spectrophotometer (JASCO, V-750). The in-line and total transmission spectra of films were measured using a UV-vis spectrophotometer (JASCO, V-750) equipped with a standard film holder (FLH-741, JASCO) and an integrating sphere (JASCO, ISV-922), respectively. PL and photoluminescence excitation (PLE) spectra of dispersions and films were obtained using a fluorescence spectrometer (JASCO, FP-8500). Absolute PLQYs were measured with a quantum efficiency measurement system (Otsuka Electronics, QE-2000-311C). The performance was evaluated for one-window LSCs with an aluminum tape background and two-window LSCs with white and black backgrounds, as shown in Fig. 1. The light guide soda glass plate (100 mm × 35 mm × 10 mm) wrapped with aluminum tape and the monocrystalline silicon (c-Si) solar cell module (35 mm × 10 mm; KIS) were assembled together. The films were attached to the region of the light guide plate without aluminum tape (35 mm × 35 mm) and illuminated with AM 1.5G simulated sunlight (1000 W m^{-2}). Current–voltage (*I–V*) curves of these devices were measured using a source meter unit (ADCMT, 6242) under AM1.5G simulated sunlight generated by a solar simulator (San-Ei Electric, XES-40S1). Spectral incident photon-to-current efficiency (IPCE) measurements were performed using a source meter unit (Keysight Technologies, B2901A) under monochromatic light irradiation (Asahi Spectra, MLS-1510). The results of the *I–V* curve and IPCE analysis were averaged five and three measurements, respectively.

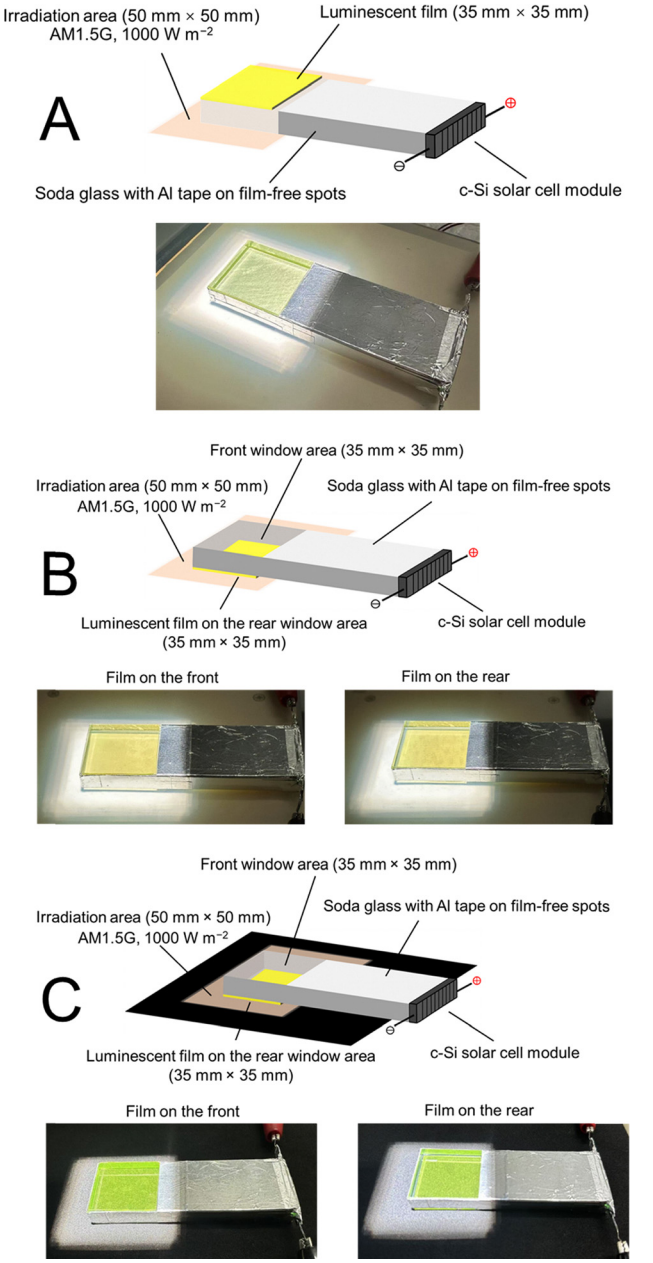

Fig. 1 Evaluation of LSC devices: (A) one-window device, (B) two-window device on the white background, and (C) two-window device on the black background.

3. Results and discussion

3.1. Comparison of properties of purified CDs and Tyr-CDs

The FE-TEM image of the purified Tyr-CDs shows that the average particle size was 32.1 ± 8.1 nm, which is larger than that of the unmodified CDs, 15.1 ± 4.4 nm, as shown in Fig. S2, SI. The dots were dark for CDs and light for Tyr-CDs. This suggests that the particles in Tyr-CDs are more loosely aggregated because of steric hindrance of tyramine on CD surface.

According to the FT-IR spectra (Fig. S3, SI), for the purified Tyr-CDs, tiny absorption peaks were observed at the same positions as those of the tyramine, which was attributed to

C–H stretching vibrations of alkyl groups (2970–2810 cm^{-1}). These peaks confirm the surface modification of CDs by tyramine. Distinct peaks of diphenyl ether were absent in the spectra of CDs and Tyr-CDs. This indicates that diphenyl ether acted as a solvent and did not react with CDs and Tyr-CDs.

As shown in Fig. S4A, SI the purified CDs and Tyr-CDs in chloroform (25 mg L^{-1}) appeared yellow and transparent under white light. Under 365 nm UV light, the yellow emission of the Tyr-CD dispersion was stronger than that of CDs to the naked eye.

Fig. S4B, SI shows the UV-vis and PL/PLE spectra of the purified CDs and Tyr-CDs in chloroform (25 mg L^{-1}). Table S1, SI, summarizes their PL/PLE properties of the purified CDs and Tyr-CDs synthesized three times and their average values. An absorption peak was observed at 470 nm, attributed to the π–π* transition between the highest occupied molecular orbital (HOMO) and the lowest unoccupied molecular orbital (LUMO) of the π-conjugated electrons.[30,33–35] The strongest excitation peak was also observed at 470 nm, with a corresponding emission peak at 550 nm. Both peaks are also attributed to the π–π* transition between the HOMO and LUMO of the π-conjugated electrons. The absorption and excitation peaks at 355 nm are possibly due to the n–π* transition of the C═N bonds which were formed by polymerization between *p*-PD molecules.[33]

The PLQYs of the purified CDs and Tyr-CDs in chloroform (25 mg L^{-1}) were measured (see Fig. S5, SI). According to Table S1, SI, the average PLQY of Tyr-CDs was 68%, being higher than that of CDs, 56%. This enhancement is attributed to the suppression of concentration quenching through π–π stacking by steric hindrance as a result of the surface modification with tyramine. This interpretation is consistent with the FE-TEM observation. The larger apparent particle size of Tyr-CDs observed in the FE-TEM images indicates a looser aggregation structure, in which the surface-bound tyramine increases the interparticle distance between sp^2 domains, effectively suppressing π–π stacking and concentration quenching.

In addition, at the same concentration of 25 mg L^{-1}, the UV-vis absorbance of the Tyr-CD chloroform dispersion was higher than that of the CD chloroform dispersion. This enhancement is possibly attributed to the increased π electron density induced by the electron-donating surface modifier, which in turn improved the PL intensity and PLQY.[30] (see Fig. S4B, SI).

3.2. Comparison of properties of CDs@EVA and Tyr-CDs@EVA films

By embedding the purified CDs and Tyr-CDs into EVA resin, CDs@EVA and Tyr-CDs@EVA films were prepared (see Table S2, SI). As shown in Fig. 2, both films were transparent under white light. The Tyr-CDs@EVA film appeared a deeper shade of yellow than the CDs@EVA film. Under 365 nm UV light, the Tyr-CDs@EVA film exhibited stronger greenish-yellow emission compared to the CDs@EVA film to the naked eye.

The in-line transmittance and in-line absorbance spectra of CDs@EVA and Tyr-CDs@EVA films are shown by solid lines in Fig. 3A and B. The CDs@EVA and Tyr-CDs@EVA films exhibited absorption peaks at 470 and 350 nm, corresponding to the π–π* and n–π* transitions, respectively. The higher absorbance and lower transmittance of the Tyr-CDs@EVA film compared to the CDs@EVA film are attributed to enhanced light absorption due to increased π electron density induced by surface modification with tyramine.

The total transmittance and total absorbance spectra measured using an integrating sphere are also shown by dashed lines in Fig. 3A and B. The difference between the in-line and total transmittances confirms the presence of light scattering, possibly caused by partially aggregated CDs and Tyr-CDs.

Fig. 3C shows the PL and PLE spectra of the CDs@EVA and Tyr-CDs@EVA films. Both films exhibited an emission peak at 540 nm and excitation peaks at 350 and 490 nm, similar to those of the purified CD and Tyr-CD chloroform dispersions. Respective Stokes shifts are 190 nm and 50 nm. The PLQY of the Tyr-CDs@EVA film was 65%, which was higher than the 49% PLQY of the CDs@EVA films, (see Fig. S6, SI and Table S2, SI). This improvement is attributed to the suppression of concentration quenching through π–π stacking by steric hindrance, as mentioned in 3.1.

3.3. Evaluation of LSCs with CDs@EVA and Tyr-CDs@EVA films under the one-window condition

The CDs@EVA and Tyr-CDs@EVA films were attached to the one window LSC with aluminum tape background (Fig. 1A). Fig. 4A shows the *I–V* curves measured under AM1.5G simulated sunlight. The short-circuit current (I_{sc}), open-circuit voltage (V_{oc}), fill factor (FF), and power conversion efficiency (η) are summarized in Table S3, SI. When the CDs@EVA and Tyr-CDs@EVA films were attached to the LSC device, I_{sc} increased from 0.842 mA to 0.988 mA and 1.084 mA by a factor of 1.17 and 1.29, respectively. As a result, η increased from 0.0226% to 0.0273% and 0.0301% by a factor of 1.21 and 1.33, respectively. Thus, the Tyr-CDs@EVA film was more effective than the CDs@EVA film. This can be explained by higher light absorption, higher PL intensity, and higher PLQY of the Tyr-CDs@EVA film.

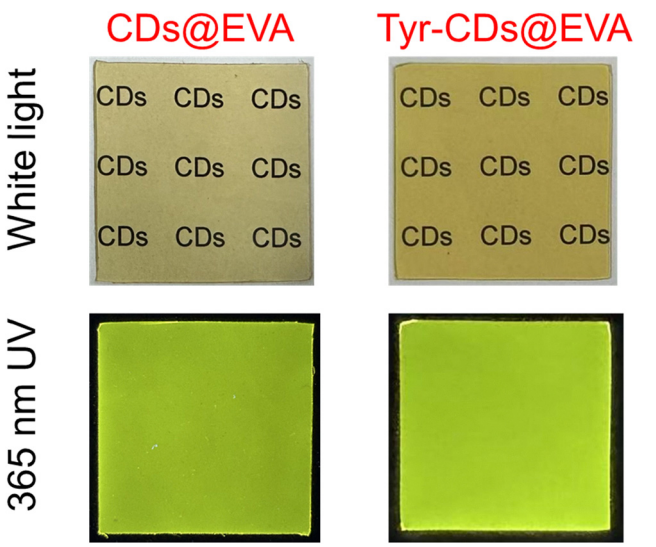

Fig. 2 Photographs of the CDs@EVA and Tyr-CDs@EVA films under the white light and 365 nm UV light.

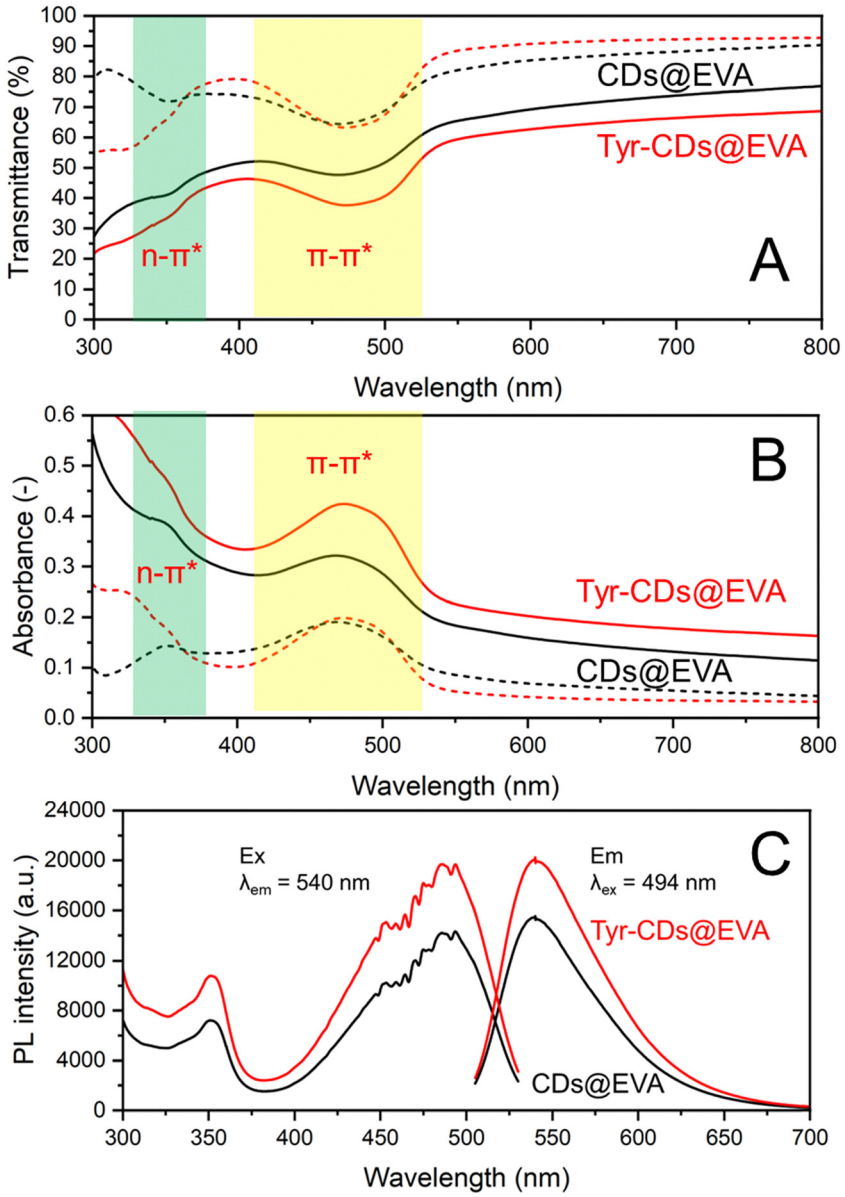

Fig. 3 (A) In-line transmittance (solid lines) and total transmittance (dashed lines) spectra and (B) in-line absorbance (solid lines) and total absorbance (dashed lines) spectra of CDs@EVA and Tyr-CDs@EVA films, (C) PL/PLE spectra of CDs@EVA and Tyr-CDs@EVA films.

As shown in Fig. 4B, the IPCEs of the LSC with CDs@EVA and Tyr-CDs@EVA films were higher than those of the LSC with no film and EVA film. This is attributed to the emission from CDs and Tyr-CDs through their absorption (excitation) by the n–π* and π–π* transitions in both the UV and visible regions, respectively; therefore, the IPCE peak wavelengths of 350 nm and 490 nm corresponds to the PLE peak wavelengths. The maximum IPCE of the Tyr-CDs@EVA film was higher than that of the CDs@EVA film, which corresponds to the trend in PL intensity.

3.4. Properties of one-window and two-window LSCs without and with each film

The EVA, CDs@EVA, and Tyr-CDs@EVA films were attached on the same LSC device in two-window setups shown in Fig. 1B and C. The *I–V* curves were measured under AM1.5G simulated sunlight as shown in Fig. 5. Table S3, SI, summarizes the I_{sc}, V_{oc}, *FF*, and η of LSC devices with no film and with EVA, CDs@EVA, and Tyr-CDs@EVA films under two-window conditions using white and black backgrounds.

As shown in Fig. 5 and Table S3, SI, Tyr-CDs@EVA film exhibited the highest I_{sc} and η, followed by CDs@EVA film, EVA film, and no film under two-window conditions with both white and black backgrounds. This trend is consistent with that observed for the one-window device shown in Fig. 4A. This is attributed to the higher PLQY and PL intensity of the Tyr-CDs@EVA film compared to those of the CDs@EVA and EVA films in the same background.

For no film, the one-window device with aluminum tape showed the higher I_{sc} and η values than the two-window device under white and black backgrounds (see Fig. S7(A) and

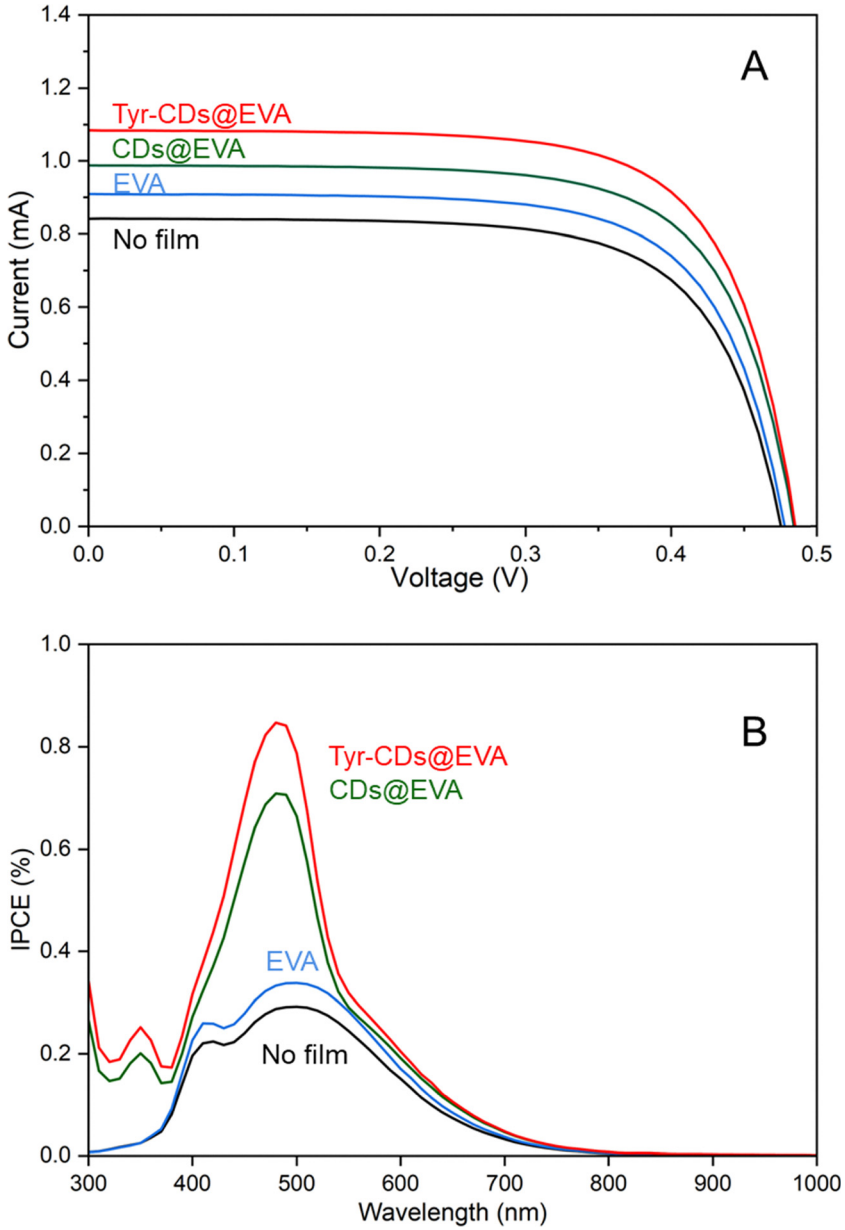

Fig. 4 (A) *I*–*V* curves and (B) IPCE spectra of the one-window LSC with no film and with EVA, CDs@EVA, and Tyr-CDs@EVA films.

Table S3, SI). This is attributed to the aluminum tape reflecting and confining more photons inside the light guide of the soda glass plate than the white and black backgrounds, resulting in more photons to enter the LSC waveguide.

The EVA film exhibited no PL emission. As a result, under the white background condition in the two-window setup when the film was attached to the front and rear sides, the I_{sc} and η values were nearly identical (see Fig. S7(B) and Table S3, SI).

For the CDs@EVA and Tyr-CDs@EVA films, the I_{sc} and η values were 0.890 mA and 0.0244%, and 0.962 mA and 0.0263%, respectively, under white background conditions in the two-window setup when the film was attached to the front side. These values were lower than 1.084 mA and 0.0301% in the one-window setup (see Fig. S7(C and D) and Table S3, SI). This is attributed to the lower reflectivity of the white background in the two-window setup compared to the aluminum tape used in the one-window rear side, as evidenced by the above-mentioned I_{sc} and η values of the devices with no film.

In contrast, under the white background in the two-window setup when the film was attached to the rear side of the LSC, the I_{sc} and η values for CDs@EVA and Tyr-CDs@EVA films were 1.071 mA and 0.0301%, and 1.246 mA and 0.0352%, respectively. These values were higher than those in the one-window setup (see Fig. S7(C and D) and Table S3, SI). This is attributed to emission in the upward and downward directions. The latter is caused by reflection from the white background. This allows more photons to enter the LSC waveguide. Furthermore, the reflection of excitation light from the white background also

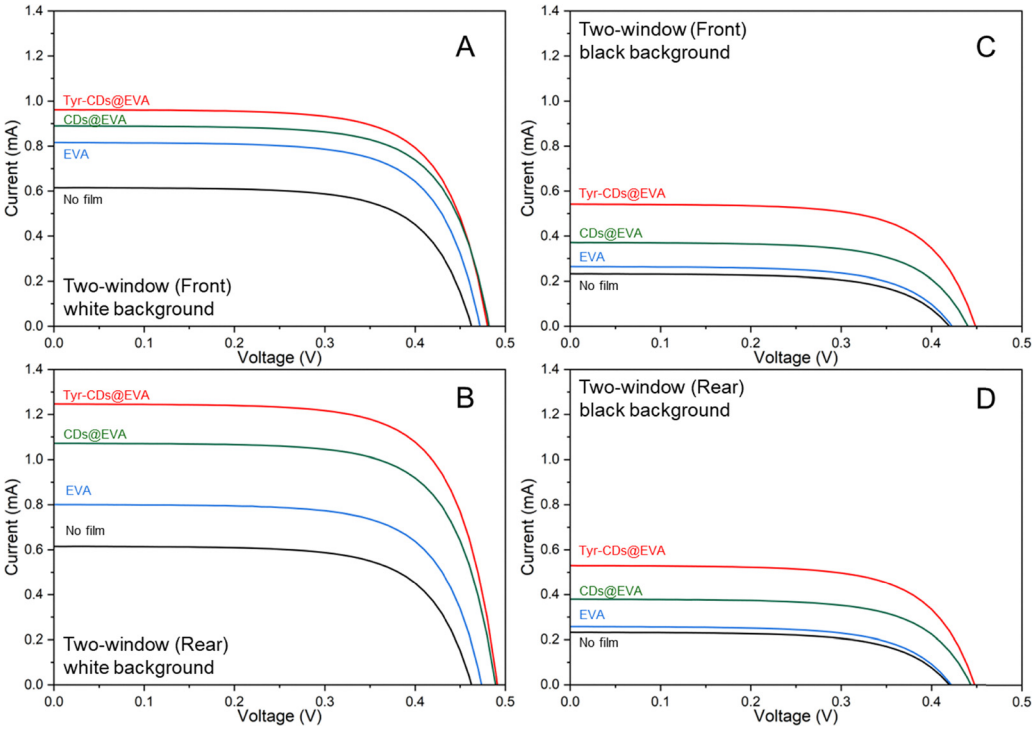

Fig. 5 *I–V* curves of the two-window LSC with no film and with EVA, CDs@EVA, and Tyr-CDs@EVA films (A) (film on the front) on the white background, (B) (film on the rear) on the white background, (C) (film on the front) on the black background, and (D) (film on the rear) on black background.

enhances emission intensity of the film. Conversely, when the CDs@EVA and Tyr-CDs@EVA films are attached to the front side of the LSC, only emission in the downward direction can enter the waveguide, while emission in the upward direction is lost.

For no film, the I_{sc} and η values under black background conditions in the two-window setup were smallest (see Fig. S7(A) and Table S3, SI), because the black background absorbs photons, reducing photon entry into the LSC waveguide. For the EVA film, when the film was attached to the front and rear sides under black background conditions in the two-window setup, the I_{sc} and η values were nearly identical (see Fig. S7(B) and Table S3, SI). This trend is consistent with that observed for the white background.

For the CDs@EVA and Tyr-CDs@EVA films, the I_{sc} and η values were 0.371 mA and 0.0088%, and 0.542 mA and 0.0133%, respectively, under black background conditions in the two-window setup when the film was attached to the front of the LSC (see Fig. S7(C and D) and Table S3, SI). These values were lower than 0.988 mA and 0.0273%, and 1.084 mA and 0.0301% in the one-window setup using CDs@EVA and Tyr-CDs@EVA, respectively. In the front-side attachment, only the emission in the downward direction enters the waveguide and the black background has low reflectance. The I_{sc} and η values for the CDs@EVA and Tyr-CDs@EVA films were 0.379 mA and 0.0091%, and 0.530 mA and 0.0129%, respectively, under black background conditions in the two-window setup when the film was attached to the rear of the LSC. These values were also lower than those in the one-window setup. In the rear-side attachment, although the film emitted in the upward and downward directions, the latter emission light and the penetrated excitation light was absorbed by the black background, resulting in photon utilization similar to that of the front-side attachment. This also indicates that most of the guided photons were confined in the soda glass by total internal reflection (TIR) and could still reach the edge solar cells, demonstrating the key contribution of TIR to maintaining LSC performance even with poor rear reflectivity.

Fig. 6 shows the IPCE spectra of the LSC device with no film and with EVA, CDs@EVA, and Tyr-CDs@EVA films under two-window conditions with both white and black backgrounds. The peak positions at 350 nm and 490 nm, respectively, and the overall IPCE intensity trends for the CDs@EVA and Tyr-CDs@EVA films are consistent with those observed for the one-window device shown in Fig. 4B. In addition, the overall IPCE intensity under the black background is lower than that under the white background (see Fig. S8), which is attributed to photon absorption by the black background.

3.5. Improved properties of LSC devices with two windows using TiO_2

Section 3.4 demonstrated that a white background enhances LSC performance by reflecting photons back into the waveguide. Thus, TiO_2 scattering functions as a reflector that can improve photon utilization. To simulate practical conditions, a black background was also employed, representing indoor environments where incident photons are absorbed, similar to light entering a room without reflection.

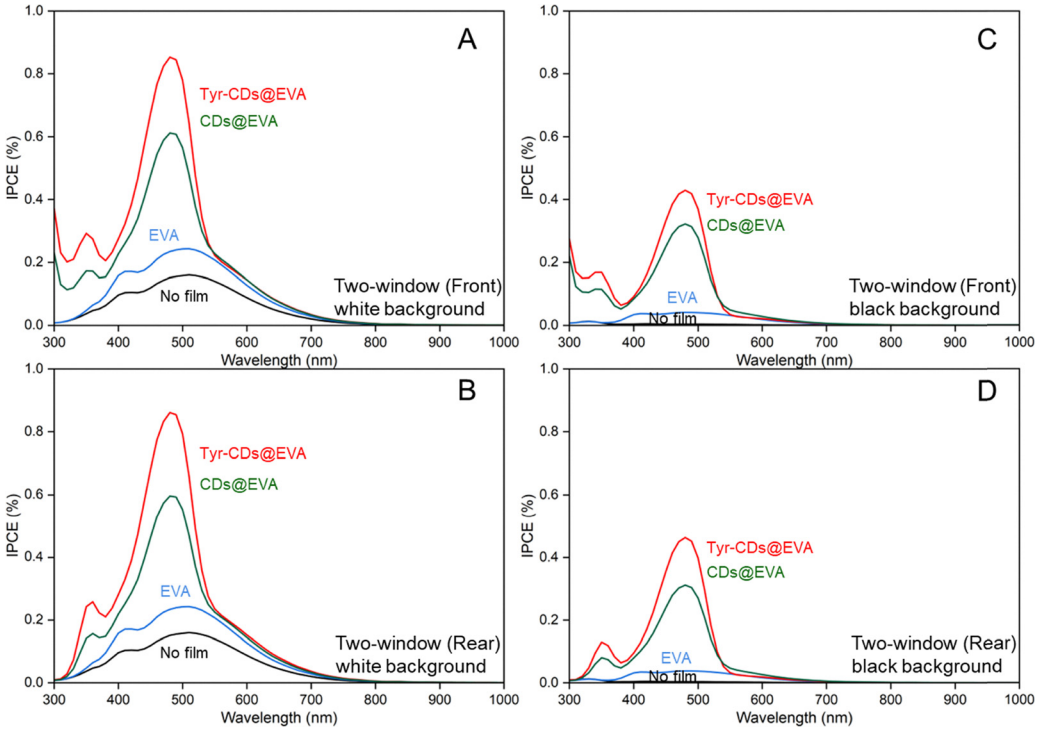

Fig. 6 IPCE spectra of the two-window LSC with no film and with EVA, CDs@EVA, and Tyr-CDsEVA films (A) (film on the front) on the white background, (B) (film on the rear) on the white background, (C) (film on the front) on the black background, and (D) (film on the rear) on the black background.

By embedding the TiO_2 nanoparticles (see Fig. S2, SI) and purified Tyr-CDs into EVA resin, The Tyr-CDs/TiO_2@EVA film, which is a double layer of Tyr-CDs@EVA and TiO_2@EVA, and the Tyr-CDs + TiO_2@EVA film, which is a single layer with both TiO_2 and Tyr-CDs uniformly dispersed in EVA, were prepared (see Table S2, SI). The photographs of the TiO_2@EVA, Tyr-CDs/TiO_2@EVA, and Tyr-CDs + TiO_2@EVA films under white light and 365 nm UV light are shown in Fig. S9, SI. Under white light, the TiO_2@EVA films appeared colorless and transparent, while the Tyr-CDs/TiO_2@EVA films appeared yellow. The increasing color intensity corresponded to enhanced scattering with higher TiO_2 concentration. The deeper yellow of the Tyr-CDs + TiO_2@EVA film indicated stronger light interaction due to volumetric scattering, which maximally increased photon absorption by the Tyr-CDs. Under 365 nm UV light, the TiO_2@EVA films showed no fluorescence. The Tyr-CDs/TiO_2@EVA films exhibited greenish-yellow emission, which enhanced with increasing TiO_2 concentration. The volumetric scattering in the Tyr-CDs + TiO_2@EVA film extended photon residence time and enhanced the probability of absorption by the Tyr-CDs, resulting in stronger PL emission than in the bottom-scattering Tyr-CDs/TiO_2@EVA structure.

The in-line transmittance and absorbance spectra of TiO_2@EVA and Tyr-CDs/TiO_2@EVA films with different TiO_2 concentrations and Tyr-CDs + TiO_2@EVA film are shown in Fig. S10 (solid lines), SI. The TiO_2@EVA films exhibited the absorption below 380 nm due to the interband transition of TiO_2. Both Tyr-CDs/TiO_2@EVA and Tyr-CDs + TiO_2@EVA films showed absorption peaks at 470 and 355 nm, corresponding to the π–π^* and n–π^* transitions of the Tyr-CDs. As the TiO_2 concentration increased, scattering was enhanced in all films, leading to decreased transmittance. The Tyr-CDs + TiO_2@EVA films exhibited the lowest transmittance and strongest photon absorption, due to volumetric scattering that extended photon residence time and increased probability of photon absorption by the Tyr-CDs.

The total transmittance and total absorbance spectra of TiO_2@EVA and Tyr-CDs/TiO_2@EVA films with different concentrations and Tyr-CDs + TiO_2@EVA film are shown in Fig. S10 (broken lines), SI. As the integrating sphere collected scattered light, the absorption below 380 nm in the total absorbance spectra of the TiO_2@EVA films was more prominent as compared to the in-line spectra. Above 380 nm in the spectra of Tyr-CDs/TiO_2@EVA and Tyr-CDs + TiO_2@EVA films, the total transmission was higher than the in-line transmission. This is because the integrating sphere detected both scattered and transmitted light.

The PL and PLE spectra of Tyr-CDs@EVA, Tyr-CDs/TiO_2@EVA and Tyr-CDs + TiO_2@EVA films are shown in Fig. S11, SI. Both Tyr-CDs/TiO_2@EVA and Tyr-CDs + TiO_2@EVA films exhibited an emission peak at 540 nm and excitation peaks approximately at 350 and 490 nm, similar to those of the Tyr-CD@EVA film and the respective Stokes shifts were 190 nm and 50 nm. With increasing TiO_2 concentration in the TiO_2@EVA layer of the Tyr-CDs/TiO_2@EVA film, enhanced scattering from TiO_2 redirected more unabsorbed photons back to the Tyr-CDs@EVA layer. This increased absorption of the Tyr-CDs, resulting in a 13% enhancement in the PL intensity compared to the Tyr-CDs@EVA film. The Tyr-CDs + TiO_2@EVA film exhibited the highest PL intensity, consistent with the greatest photon

absorption. This represents a 43% enhancement in the PL intensity.

However, in the UV region, the PL intensity in the excitation spectrum of the Tyr-CDs + TiO_2@EVA film was lower than those of the Tyr-CDs/TiO_2@EVA and Tyr-CDs@EVA films due to significant UV absorption through the interband transition of TiO_2, which reduced photon availability for excitation. In contrast, the PL intensities in the UV region of the excitation spectra for the Tyr-CDs/TiO_2@EVA films were similar to that for the Tyr-CDs@EVA film, because the top layer of Tyr-CDs@EVA absorbed most of UV light before it reached the bottom layer of TiO_2@EVA.

The PLQYs of the Tyr-CDs/TiO_2@EVA films containing 0.05, 0.10, and 0.15 wt% of TiO_2 and the Tyr-CDs + TiO_2@EVA film were 64%, 60%, 60%, and 64%, respectively (Table S2, SI). These values are generally consistent with that of the Tyr-CDs@EVA film (64%). The LSC efficiency, η, in the double-layer configuration increased from 0.0134% to 0.0145% with increasing the TiO_2 concentration from 0.05 wt% to 0.15 wt% (see Table S3, SI), although the PLQY slightly decreased from 64% to 60%. This indicates that TiO_2-induced light scattering plays a more important role in determining the device performance than these minor decrease in the PLQYs of films.

The Tyr-CDs/TiO_2@EVA and Tyr-CDs + TiO_2@EVA films were attached on the same LSC device in two-window setup (rear side) as shown in Fig. 1C. The *I–V* curves measured under AM1.5G simulated sunlight were shown in Fig. 7(A). Table S3,

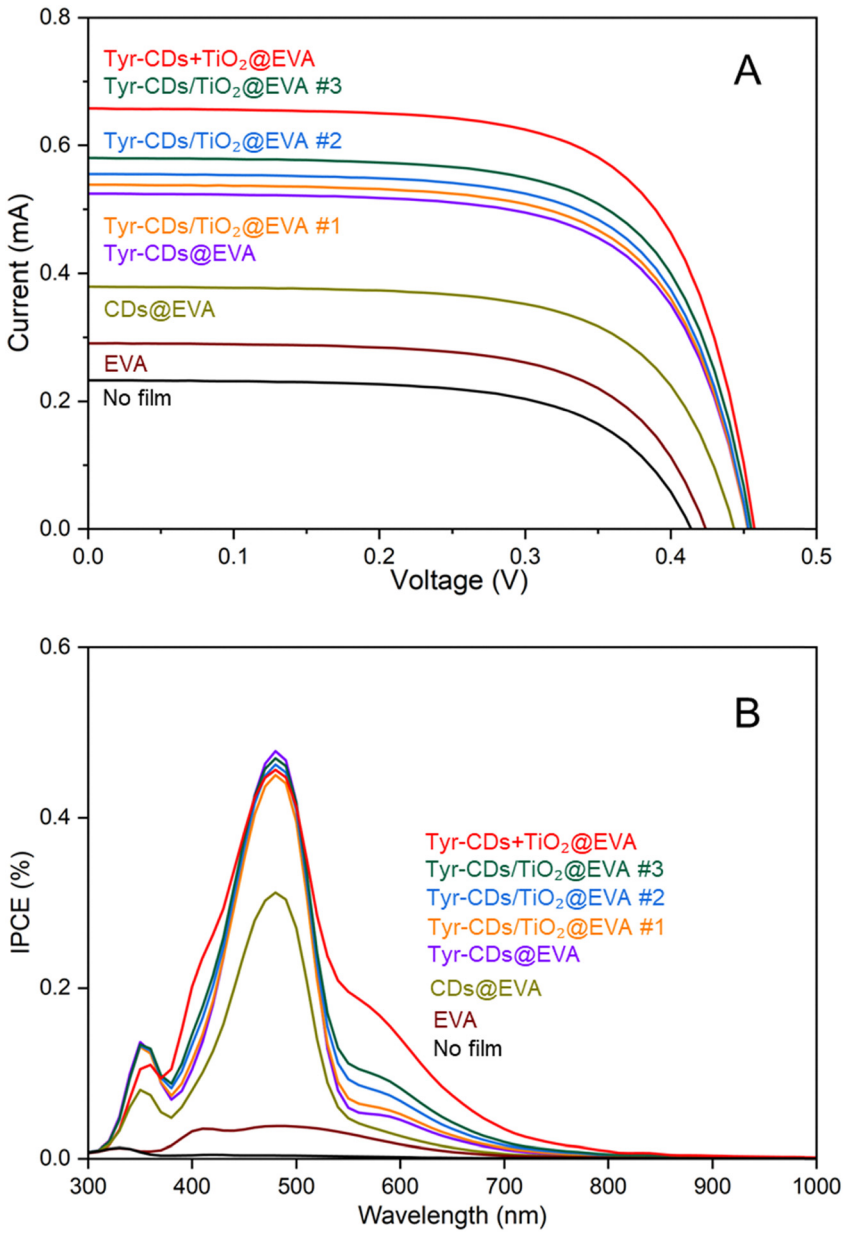

Fig. 7 (A) *I–V* curves and (B) IPCE spectra of the two-window LSC with no film and with EVA, CDs@EVA, Tyr-CD@EVA, Tyr-CDs/TiO_2@EVA, and Tyr-CDs + TiO_2@EVA films on the rear under the condition of the black background.

Table 2 Comparison of the optical properties and power conversion efficiency of the same soda glass-based LSC device with different luminescent materials evaluated under the same conditions

Luminescent material	Absorption edge (nm)	Main PL Peak (nm)	PLQY (%)	η/η (no film) (%)	Ref.
Under the one-window condition					
$CuGaS_2$/ZnS@EVA	~450	568	70	196	37
$CsPbCl_3$:Mn^{2+},Er^{3+}@EVA	~410	600	73	118	38
CDs@EVA	~530	540	49	119	33
Tyr-CDs@EVA	~530	540	65	133	This work
Under the two-window condition with a black background					
Tyr-CDs + TiO_2@EVA	~530	540	64	327	This work

SI, summarizes the I_{sc}, V_{oc}, *FF*, and η of LSC devices with Tyr-CDs/TiO_2@EVA and Tyr-CDs + TiO_2@EVA films under two-window conditions using black backgrounds. The Tyr-CDs + TiO_2@EVA film exhibited the strongest light scattering among all samples, which maximized the absorption efficiency of the Tyr-CDs due to volumetric scattering, resulting in the highest LSC efficiency. Meanwhile, the Tyr-CDs/TiO_2@EVA #3 film showed the strongest scattering among the Tyr-CDs/TiO_2@EVA films, resulting in the highest LSC efficiency.

Fig. 7(B) shows the IPCE spectra of the LSC devices with Tyr-CDs + TiO_2@EVA film, Tyr-CDs/TiO_2@EVA films and Tyr-CDs@EVA film under the two-window condition (rear side) with black background. The peak positions appeared at 350 and 490 nm, respectively. Beyond 530 nm, the IPCE enhancement was mainly attributed to light scattering.[33] The Tyr-CDs + TiO_2@EVA film showed the strongest light scattering, resulting in the largest enhancement, followed by Tyr-CDs/TiO_2@EVA films #3, #2, and #1, consistent with the above-mentioned light scattering results. Below ~380 nm, the IPCE value of the Tyr-CDs + TiO_2@EVA film was lower than those of the other films due to the absorption by TiO_2. It should be noted that excessive light scattering can cause photons to escape from the waveguide, resulting in energy loss. In this study, this effect was not significant for the TiO_2 concentration up to 0.15 wt%. However, further increasing the TiO_2 concentration may cause light to escape from the waveguide due to over-scattering.

Finally, Table 2 shows a comparison of LSC devices fabricated with the same soda glass-based configuration originally designed in our group. The same LSC setup has been consistently employed in all our previous works to evaluate device performance using identical characterization methods. Under the one-window condition, the LSC with $CuGaS_2$/ZnS@EVA achieved the highest η/η (no film) (%) of 196%,[37] where η/η (no film) (%) represents the relative power conversion efficiency compared with the device without a film. This high value can be attributed to the high PLQY (70%) and large Stokes shift, resulting in negligible self-absorption. The η/η (no film) (%) of the $CsPbCl_3$:Er^{3+},Mn^{2+}@EVA was 118%[38] because of the low QD concentration of 0.19 wt% in an EVA film, even though the film exhibited the highest PLQY (73%). For CDs@EVA, the η/η (no film) (%) was 119% due to its relatively low PLQY (49%) and partial spectral overlap between absorption and emission, which caused partial self-absorption losses.[33] In contrast, Tyr-CDs@EVA increased η/η (no film) (%) from 119% to 133%, mainly because the PLQY increased from 49% to 65%, leading to improved power conversion efficiency.

Under the two-window condition with a black background, Tyr-CDs + TiO_2@EVA showed a η/η (no film) (%) of 327%. This condition simulates real sunlight passing through a window into an indoor environment. The Tyr-CDs + TiO_2@EVA film, which has a higher PLQY and strongest light scattering ability, demonstrated a significant enhancement in power conversion efficiency.

4. Conclusions

Tyramine modification of CDs at 250 °C for 0.5 h under ambient conditions increased the PLQY from 56% to 68% after centrifugation and purification, which is attributed to the suppression of concentration quenching through π–π stacking by steric hindrance and possibly to the increased π electron density induced by the electron-donating surface modifier. Embedding Tyr-CDs into EVA produced Tyr-CDs@EVA films with enhanced optical absorption, PL intensity, and PLQY compared with CDs@EVA films. When applied to LSC devices under the one-window condition, the I_{sc} and η enhancement factors increased from 1.17 to 1.29 and from 1.21 to 1.33, respectively, due to surface modification. Furthermore, incorporating TiO_2 nanoparticles into the EVA matrix as scattering films or uniformly dispersing them in the Tyr-CDs@EVA film improved photon utilization and LSC performance. This was achieved by enhancing visible light scattering and promoting photon absorption by Tyr-CDs. The Tyr-CDs + TiO_2@EVA film showed the highest performance due to volumetric scattering, which uniformly redirected more photons of excitation light and emission light. This simple and green modification strategy improved the intrinsic optical properties of CDs and demonstrated that the combining them with low-cost TiO_2 nanoparticles provides an efficient way to enhance visible-light utilization in LSCs. In this system, TiO_2 primarily functions as a scattering medium, and the photocatalytic activity under visible-light excitation is negligible.[36] These results offer valuable insights for the practical application of CD-based luminescent solar concentrators.

In addition, Fig. S12, SI shows the photostability of CDs and Tyr-CDs in chloroform and in EVA-based films under continuous irradiation. The lower photostability of Tyr-CDs compared with CDs is mainly attributed to the former having stronger absorption at the excitation wavelength, resulting in promoted photo-oxidation. This effect is most pronounced in the Tyr-CDs + TiO_2@EVA film, where TiO_2-induced light scattering enhances photon utilization and leads to the fastest photobleaching among the evaluated films. Future research could focus on improving the photostability of Tyr-CDs by applying advanced LSC encapsulation processes to prevent air and moisture from penetrating the films, or by embedding Tyr-CDs in silica nanoparticles to suppress surface oxidation.[40]

Author contributions

Y. L.: formal analysis, investigation, methodology, writing – original draft; Y. I.: supervision, writing – review and editing; T. I.: conceptualization, project administration, supervision, writing – review and editing. All authors gave final approval for publication and agreed to be held accountable for the work performed therein.

Conflicts of interest

There are no conflicts to declare.

Data availability

Additional data used for the study are available from the corresponding authors upon reasonable request.

The authors declare that all data supporting the results reported in this study are available within the paper and the supplementary information (SI). Supplementary information is available. See DOI: https://doi.org/10.1039/d5tc03684d.

Acknowledgements

This work was supported by JST SPRING, Japan Grant Number JPMJSP2123.

References

1 B. S. Richards and I. A. Howard, *Energy Environ. Sci.*, 2023, **16**, 3214–3239.
2 K. Jo and H. J. Kim, *Appl. Sci. Converg. Technol.*, 2021, **30**, 14–20.
3 S. Castelletto and A. Boretti, *Nano Energy*, 2023, **109**, 108269.
4 M. A. Hernández-Rodríguez, S. F. H. Correia, R. A. S. Ferreira and L. D. Carlos, *J. Appl. Phys.*, 2022, **131**, 140901.
5 F. Mateen, S. Y. Lee and S.-K. Hong, *J. Mater. Chem. A*, 2020, **8**, 3708–3716.
6 W. E. Benjamin, D. R. Veit, M. J. Perkins, E. Bain, K. Scharnhorst, S. McDowall, D. L. Patrick and J. D. Gilbertson, *Chem. Mater.*, 2014, **26**, 1291–1293.
7 M. J. Currie, J. K. Mapel, T. D. Heidel, S. Goffri and M. A. Baldo, *Science*, 2008, **321**, 226–228.
8 A. R. Frias, M. A. Cardoso, A. R. Bastos, S. F. Correia, P. S. André, L. D. Carlos, V. de Zea Bermudez and R. A. Ferreira, *Energies*, 2019, **12**, 451.
9 I. Motta, G. Bottaro, M. Rando, M. Rancan, R. Seraglia and L. Armelao, *J. Mater. Chem. A*, 2024, **12**, 22516–22527.
10 J.-C. G. Bünzli, *Chem. Rev.*, 2010, **110**, 2729–2755.
11 U. Resch-Genger, M. Grabolle, S. Cavaliere-Jaricot, R. Nitschke and T. Nann, *Nat. Methods*, 2008, **5**, 763–775.
12 F. Meinardi, S. Ehrenberg, L. Dhamo, F. Carulli, M. Mauri, F. Bruni, R. Simonutti, U. Kortshagen and S. Brovelli, *Nat. Photonics*, 2017, **11**, 177–185.
13 H. Zhao, Y. Zhou, D. Benetti, D. Ma and F. Rosei, *Nano Energy*, 2017, **37**, 214–223.
14 L. J. Brennan, F. Purcell-Milton, B. McKenna, T. M. Watson, Y. K. Gun'ko and R. C. Evans, *J. Mater. Chem. A*, 2018, **6**, 2671–2680.
15 R. Terricabres-Polo, T. A. de Bruin, A. Kaul, W. G. van Sark and C. D. M. Donega, *Adv. Energy Mater.*, 2024, **14**, 2402375.
16 S. N. Baker and G. A. Baker, *Angew. Chem., Int. Ed.*, 2010, **49**, 6726–6744.
17 H. Li, Z. Kang, Y. Liu and S.-T. Lee, *J. Mater. Chem.*, 2012, **22**, 24230–24253.
18 T. Mandal, S. R. Mishra, M. Kumar and V. Singh, *Sustainable Energy Fuels*, 2024, **8**, 5638–5671.
19 W. Li, X. Wang, J. Lin, X. Meng, L. Wang, M. Wang, Q. Jing, Y. Song, A. Vomiero and H. Zhao, *Nano Energy*, 2024, **122**, 109289.
20 Y. Li, P. Miao, W. Zhou, X. Gong and X. Zhao, *J. Mater. Chem. A*, 2017, **5**, 21452–21459.
21 J. Li, H. Zhao, X. Zhao and X. Gong, *Nanoscale*, 2021, **13**, 9561–9569.
22 A. Cayuela, M. Soriano, C. Carrillo-Carrión and M. Valcárcel, *Chem. Commun.*, 2016, **52**, 1311–1326.
23 H. Peng and J. Travas-Sejdic, *Chem. Mater.*, 2009, **21**, 5563–5565.
24 M. Wu, Y. Wang, W. Wu, C. Hu, X. Wang, J. Zheng, Z. Li, B. Jiang and J. Qiu, *Carbon*, 2014, **78**, 480–489.
25 D. Shen, Y. Long, J. Wang, Y. Yu, J. Pi, L. Yang and H. Zheng, *Nanoscale*, 2019, **11**, 5998–6003.
26 S. Liang, M. Wang, W. Gao and X. Zhao, *Opt. Mater.*, 2022, **128**, 112471.
27 H. Ren, Y. Chen, A. Labidi, K. Zhao, X. Xu, S. I. Othman, A. A. Allam, H. A. Rudayni and C. Wang, *Int. J. Biol. Macromol.*, 2024, **273**, 133118.
28 T. Chu, X. Yang, M. Chen, Q.-S. Shi, X. Xie and Y. Guo, *Green Chem.*, 2024, **26**, 2773–2782.
29 F. Yuan, Y.-K. Wang, G. Sharma, Y. Dong, X. Zheng, P. Li, A. Johnston, G. Bappi, J. Z. Fan and H. Kung, *Nat. Photonics*, 2020, **14**, 171–176.
30 K. Sato, R. Katakami, Y. Iso and T. Isobe, *ACS Appl. Nano Mater.*, 2022, **5**, 7664–7669.
31 M. Polché, B. F. José Miguel, C. A. Guzmán González, G. González Contreras and V. H. Romero Arellano, *Nanomaterials*, 2023, **13**, 2480.
32 Y. Jiang and F. Zhao, *Front. Energy Res.*, 2021, **9**, 682709.
33 Y. Liu, Y. Iso and T. Isobe, *J. Mater. Chem. C*, 2025, **13**, 786–792.
34 R. Sato, Y. Iso and T. Isobe, *Langmuir*, 2019, **35**, 15257–15266.
35 K. Washio, K. Sato, Y. Iso and T. Isobe, *ECS J. Solid State Sci. Technol.*, 2023, **12**, 076001.
36 S. G. Kumar and L. G. Devi, *J. Phys. Chem. A*, 2011, **115**, 13211–13241.
37 S. Hase, Y. Iso and T. Isobe, *J. Mater. Chem. C*, 2022, **10**, 3523–3530.
38 P. Song, S. Hase, S. Zhao, Z. Xu, Y. Iso and T. Isobe, *ACS Appl. Nano Mater.*, 2022, **5**, 2522–2531.
39 Y. Ochi, A. Otani, R. Katakami, A. Ogura, K. Takao, Y. Iso and T. Isobe, *J. Mater. Chem. C*, 2024, **12**, 6548–6558.
40 L. F. Ornelas-Hernández, A. Garduño-Robles and A. Zepeda-Moreno, *Nanoscale Res. Lett.*, 2022, **17**, 56.

